Full-scale Cold-bent Glass Breaking Tests with Various Parameters

Katsuto Tomoeda, Yuriko Okamoto

ASAHI BUILDING-WALL CO., Ltd., Japan
katsuto-tomoeda@agb.co.jp; yuriko-okamoto@agb.co.jp

Abstract

Cold-bent glass is one method of achieving free-form shapes and has the advantages of high optical quality and low environmental load compared to heat-bent glass. Although many studies have been conducted on cold-bent glass, there are few examples of comprehensive investigations of full-scale glass bending up to fracture. In this study, single-corner cold-bending tests were conducted with full-size laminated glass (GH3040xGW1840) in a configuration similar to an actual installation in a vertical set-up. The parameters were supporting-method, glass-thickness and interlayer-type. After that, a wind-load test was also conducted. In the case of 4-line-support, the peak maximum-principal-stress was generated around the middle of the long edge. In the case of point-supports, the peak value was generated around the loading-point and the diagonal support-point. Regarding 6-point-support, the stresses around the middle support-points weren't large. For the same amount of bending, the reaction force increased in proportion to the glass-thickness (e.g. 8mm, 10mm), but the increase in stress was small, indicating that the effect of glass-thickness isn't large. When exceeding a certain amount of bending, a buckling-phenomenon occurred. That was earlier in thinner glass. The glass fracture origins were in high maximum-principal-stress area. When the interlayer-type was SentryGlas (SG), the stresses and reaction forces were larger than those of PVB. An ideal uniform-load of up to ±4.5 kPa was applied to the glass in the cold-bent state using an air-pressure chamber. The effect of cold-bent was added, with a slight distortion of the stress distribution. Also, FEAs were conducted for each test to confirm the validity of the analysis model and to perform further studies. Cold-bent stress at the middle of the long edge under 4-line-support depend on the sizes of width, height and thickness of glass specimen. A series of tests and analyses confirmed the results of previous studies.

Keywords

Cold-bent glass, full-scale, breaking test, various parameters, laminated glass

Article Information

- Published by Glass Performance Days, on behalf of the author(s)
- Published as part of the Glass Performance Days Conference Proceedings, June 2025
- Editors: Jan Belis, Christian Louter & Marko Mökkönen
- This work is licensed under a Creative Commons Attribution 4.0 International (CC BY 4.0) license.
- Copyright © 2025 with the author(s)

1. Introduction

Cold-bent glass is obtained by forcibly deforming a single corner of flat glass in the out-of-plane direction. It is one of the technologies that has been attracting attention in Japan, with recent examples of “Japan Sport Olympic Square (2019)” and “Toranomon Hills GLASS ROCK (2024).” It can produce a three-dimensional bent shape without the application of heat and offers multiple advantages in terms of environmental impact, cost, workability, and optical qualities. However, bending glass causes long-term residual stress and limits the range of shapes that can be bent. To understand these issues, full-size specimens were prepared in a configuration similar to an actual vertical installation and tested to failure. Tests were conducted with different boundary conditions, glass thicknesses, and interlayer types. In addition, a wind load test was conducted using a 4-line support specimen to understand the behavior of cold-bent glass under wind load. Finally, using the validated FEA models, various specimen patterns with different glass thicknesses, heights, and widths were prepared, and the equation of bending displacement corresponding to edge-generated stress was calculated and evaluated.

2. Cold-bent tests and analyses

In this section, the behavior of laminated glass specimens under cold-bent states was investigated to clarify the safe usage of cold-bent glass. Tests and analyses were performed using specimens with variable patterns to confirm the fracture states. And the effects of the differences between the specimens were evaluated.

2.1. Outline

- Outline of the test
  Fig. 1 shows the test setup of a 4-line-support specimen as an example. The laminated glass specimen GW1840 x GH3040 was set vertically on the steel frame. The out-of-plane displacements were fixed at points A, B, and D, with points B and D serving as ball-joint supports that are rotatable in three axial directions. Point C was the loading point and was pulled in the out-of-plane interior direction. Loading point C is in the same position as the corner of glass when viewed from the elevation view. The diagonal AC, which contains the loading point C, is defined as the “loading-axis,” and the other diagonal BD is defined as the “transverse-axis.” The out-of-plane deflections at the centers of both axes are defined as “sag” S_L and S_T, respectively.

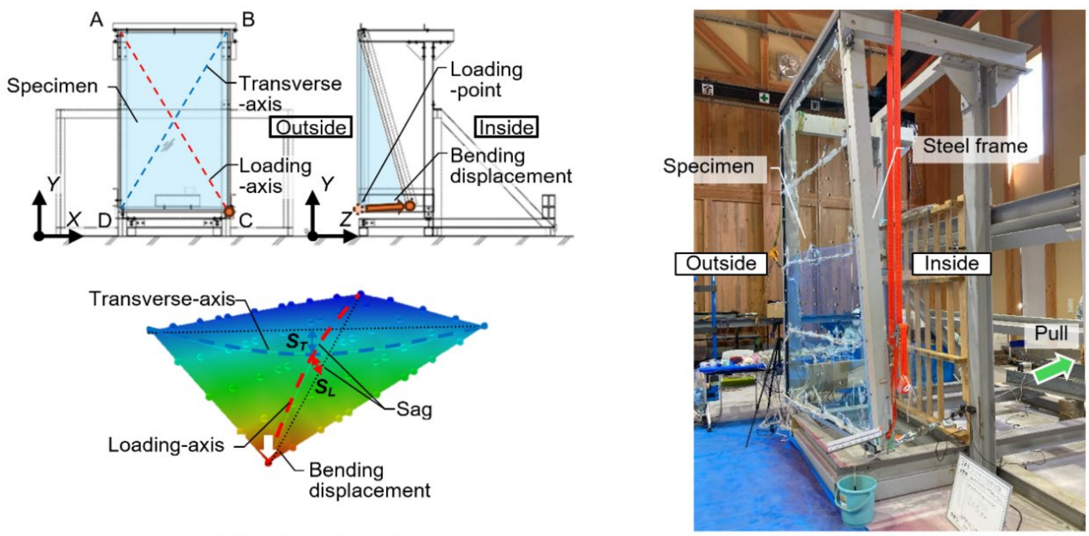

(a) Specimen image *(b) Specimen photo*

Fig. 1: Test setup.

Table 1 shows the series of specimens tested. There are three types of support conditions (4-line-support / 4-point-support / 6-point-support), two types of glass thicknesses (HS8 / HS10), and two types of interlayers (SG / PVB). Four specimens (No. 2, 4, 5, and 6) were deformed up to failure, and the condition after failure was observed. Also, FEAs were conducted for these four specimens to validate the FEA models. The support conditions of the specimens are shown in Fig. 2. Heat-strengthened laminated glass was used for all the specimens. The thickness of the interlayer was 60 mils for all. The test specimens were made with an aluminum sash for the 4-line-support and a steel point support for the point-supports. The width of the rubber for the 4-line-support was 9 mm, and the size of the rubber for the point-supports was 40 mm x 40 mm.

Table 1: Series of specimens.

No.	Support	Glass thickness	Interlayer	Final State	FEA conducted
1	4-line-support	HS8 + HS8	SG60mil	Unbreak *D*=150mm	-
2	4-line-support	HS8 + HS8	PVB60mil	Break *D*=340mm	○
3	4-line-support	HS10 + HS10	SG60mil	Unbreak *D*=150mm	-
4	4-line-support	HS10 + HS10	PVB60mil	Break *D*=400mm	○
5	4-point-support	HS8 + HS8	SG60mil	Break *D*=430mm	○
6	4-point-support	HS10 + HS10	SG60mil	Break *D*=330mm	○
7	6-point-support	HS8 + HS8	SG60mil	Unbreak *D*=150mm	-
8	6-point-support	HS10 + HS10	SG60mil	Unbreak *D*=150mm	-

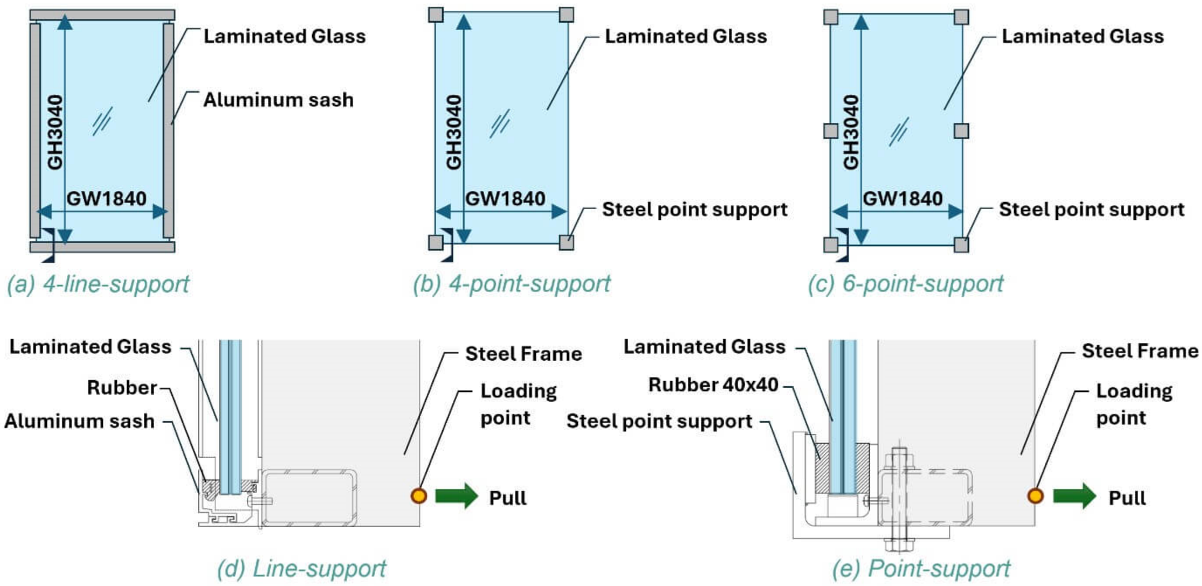

Fig. 2: Supporting condition of the specimens.

- Measurement methods
  The measurement positions of strain and displacement are shown in Fig. 3. The strain generated in the glass was measured using a triaxial strain gauge. In the following sections, the analysis will focus on measurement points No. 10 and No. 11 as representative points of the center-of-edge and center-of-plane stresses, respectively. Deformation on the exterior side of the glass was measured using a motion capture system. To accurately observe the deformed shape, as many measurement markers as possible were placed along both the loading-axis and transverse-axis. A load cell was attached to the loading point C, and the reaction force was measured. By attaching a steel wire to the load cell and pulling it with a jack, bending displacement was applied in the out-of-plane interior direction at 10 mm intervals until the glass fractured.

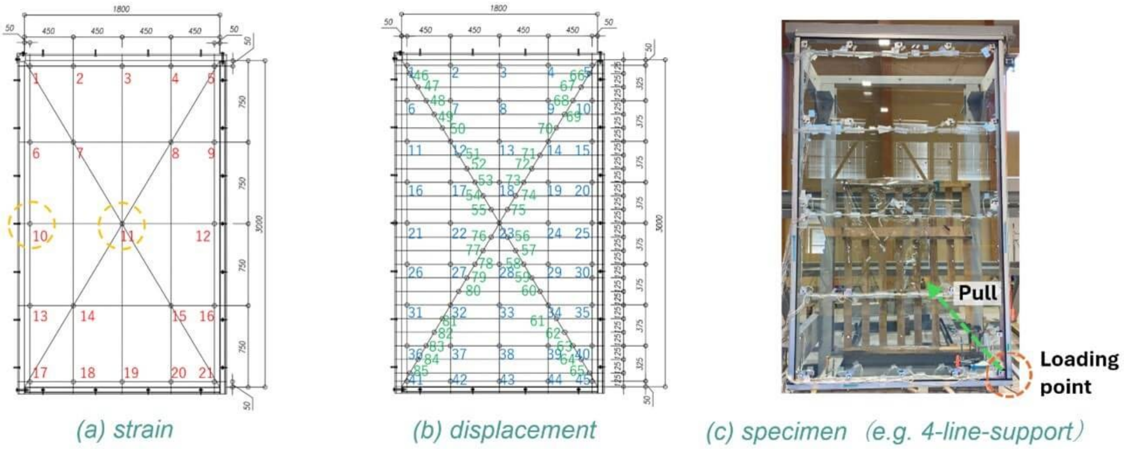

Fig. 3: Measurement position.

- Outline of the analysis
  Fig. 4 shows the FEA model used in the tests (e.g., 4-line-support specimen). FEAs were conducted using “PTC Creo Simulate 9.0,” considering geometric nonlinearity for large deformations. Laminated glass, rubber, sealing, frames, and sashes were modeled with solid elements. For the laminated glass, the interlayer PVB was modeled with stiffness values set based on temperature and load duration. The boundary conditions were set with two fixed edges, AB and AD. At points B and D, the steel frame was pin-connected. A loading point was set at point C to apply a bending displacement in the out-of-plane interior direction Z. Point C can move freely to direction X and Y and fully rotatable around three axial directions.

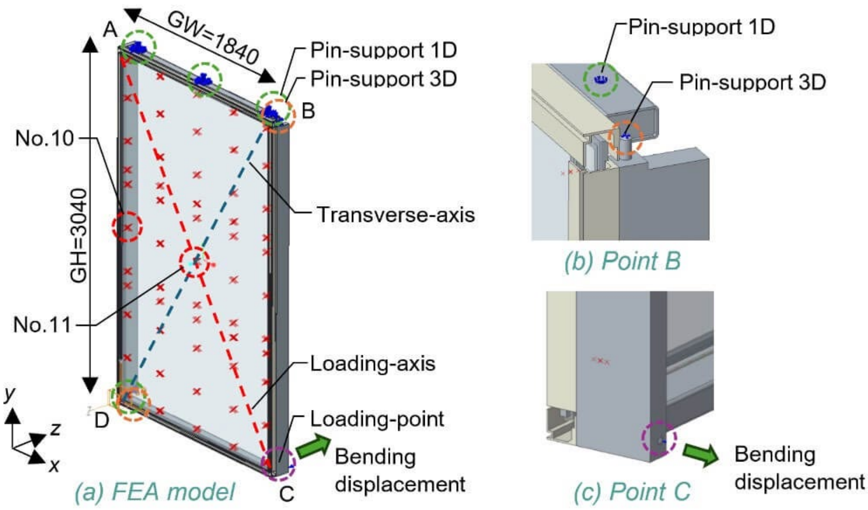

Fig. 4: FEA model.

2.2. Result

- Breaking state
  Fig. 5 shows specimens No. 2, 4, 5, and 6 after fracture. In all the specimens, the inner and outer glass surfaces broke simultaneously at a certain moment as the bending displacement increased, and cracks were observed over the entire glass surface. Cracks on the outer surface ran nearly perpendicular to the loading-axis, while those on the inner surface ran nearly perpendicular to the transverse-axis corresponding to the saddle-shape of glasses. The directions of cracks were similar to those obtained from the test result of Van Driel et al. (2022) in the sense that the paths of the cracks corresponded to the deformed shape of glass. For the 4-line-support configuration, a fracture origin was observed near the center of the long edge opposite the loading point C. For the 4-point-support configuration, a fracture origin was observed near the steel point support opposite the loading point C. The fracture origins were in the plane 20–30 mm from the edge. For the 4-point-support specimen (HS10), no fracture origin could be found. A mirror surface was observed at the fracture origin using a microscope. The mirror radius R_m was approximately 1.2–1.3 mm, and the estimated fracture stress σ_e calculated by the experimental equation (1) was 50–52 MPa. This value was close to the average breaking stress of 70.6 MPa for heat-strengthened glass, as specified in the Japanese guidelines.

$$\sigma_e = 580/\sqrt{R_m} \times 0.098 \qquad (1)$$

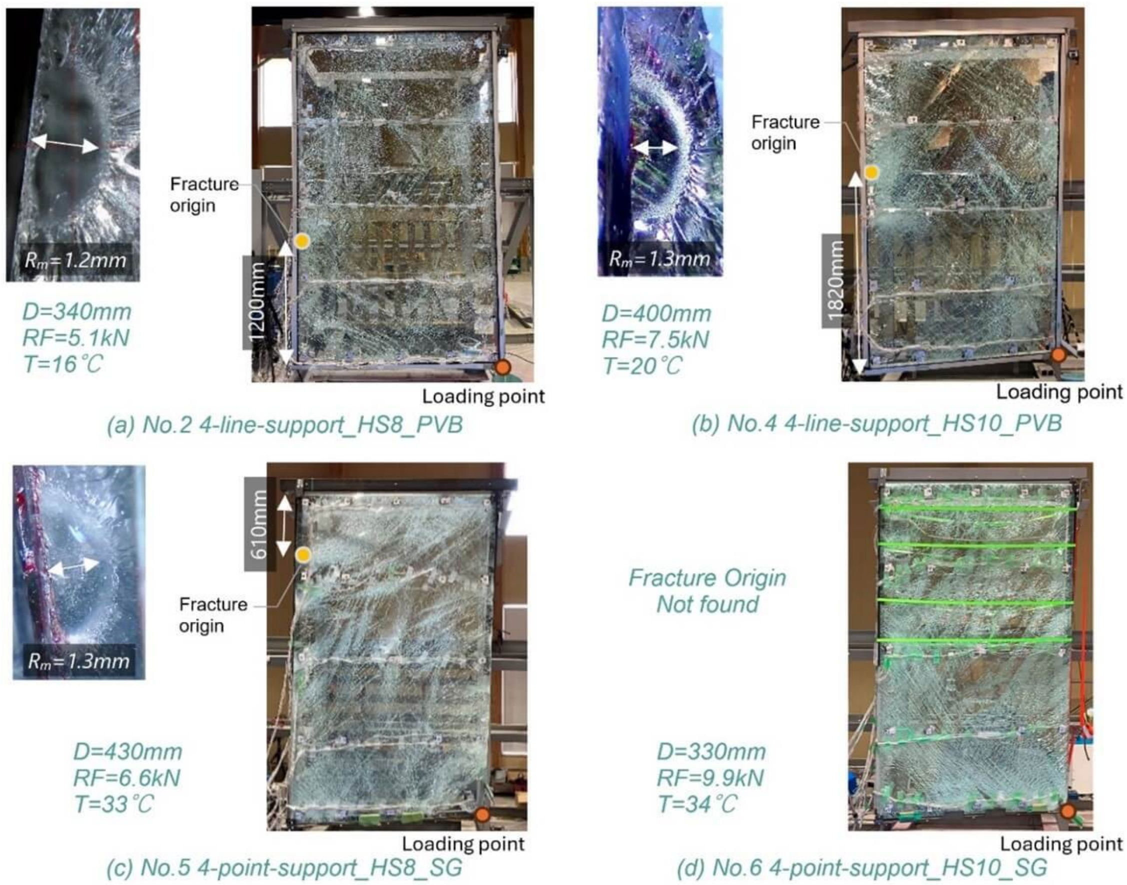

Fig. 5: Breaking state.

- Deformation, stress, and reaction force of the tests
  The displacement distribution of the edges is shown in Fig. 6. In the case of 4-line-support, the out-of-plane deformation was constrained in the sash taking an S-shape and had a small value. In the case of 4-point-support, the long edge was significantly deformed out-of-plane in an arc shape, as the edge was free. Fig. 7 shows the bending displacement–sag relationship and the bending displacement–

maximum principal stress relationship. In the case of 4-line-support, the loading and transverse axes of HS10 follow approximately the same path, but in HS8, the path branches after the bending displacement exceeds 100 mm: the sag of the loading-axis becomes larger than that of the transverse-axis, and the shape collapses asymmetrically. Similarly, in the case of 4-point-support, branching occurred when the bending displacement exceeded 100 mm for both HS8 and HS10; branching was more pronounced for HS8. It was found that the smaller the plate thickness and the fewer the constraints imposed by the boundary conditions, the more likely the shape was to collapse asymmetrically. The maximum principal stress at the center of the plane exhibited a branching pattern similar to that observed for the sag. This is a buckling phenomenon as noted by Staaks (2003) and can be explained by the fact that when the radius of curvature of the axis becomes larger (smaller), the sag becomes smaller (larger) and the maximum principal stress becomes smaller (larger), as shown in Fig. 8, in which the case of transverse-axis buckling is shown. However, the maximum principal stress values at the edges show that the branching is less pronounced than that at the center of the plane, and the effect of the non-linearities was small. The branching indicates that bending is occurring, so the edges experience less bending stress and greater tensile stress compared to the center of the plane, where bending occurs after buckling. In terms of the fracture moment, the maximum principal stress of each specimen is between the estimated fracture stress of 50–52 MPa and the average breaking stress of 70.6 MPa. For the reaction force, the thicker the glass, the larger the reaction force (as shown in Fig. 9) in both the 4-line-support and 4-point-support specimens. The 4-point-support specimens exhibited a larger reaction force compared with that of the 4-line-support specimens. This is considered to be as a result of the interlayer stiffness, as SG is much stiffer than PVB.

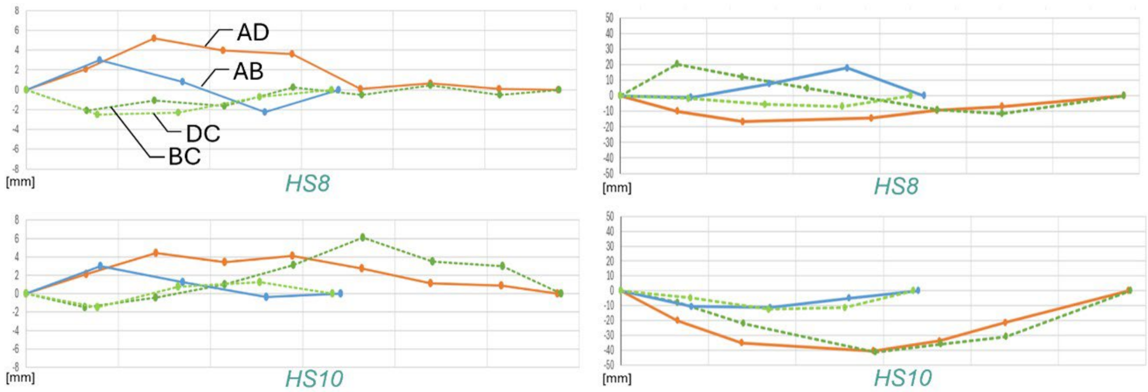

(a) 4-line-support (PVB) *(b) 4-point-support (SG)*

Fig. 6: Out-of-plane deformation of glass edges.

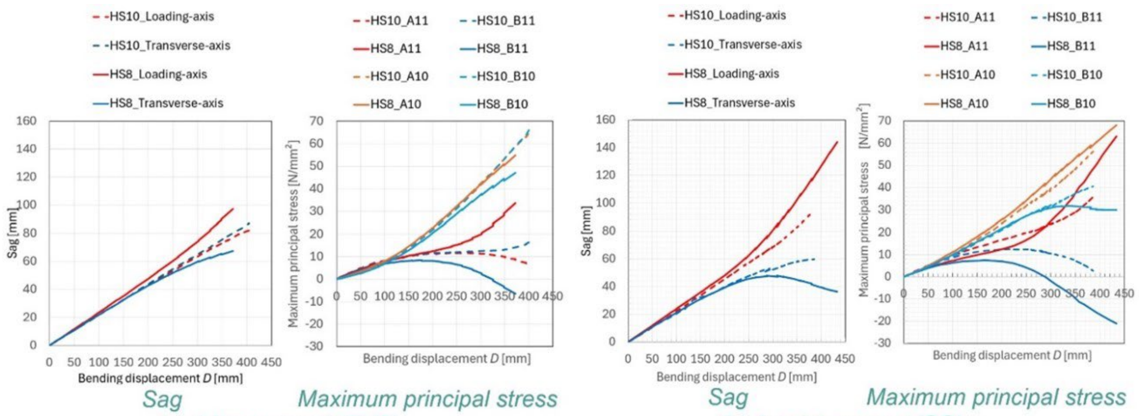

(a) 4-line-support (PVB) *(b) 4-point-support (SG)*

Fig. 7: Sag and maximum principal stress against bending displacement (glass thickness comparison).

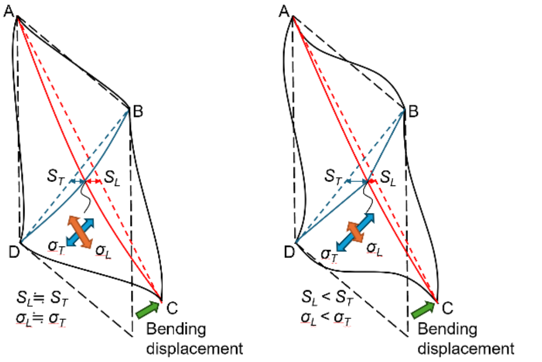

(a) Before buckling *(b) Buckling of transverse-axis*

Fig. 8: Buckling model

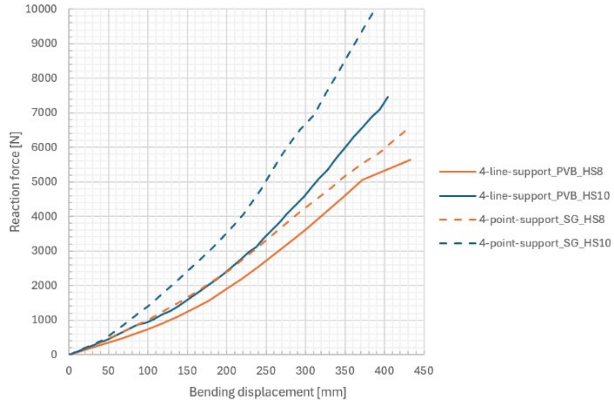

Fig. 9: Bending displacement – reaction force relationship

- Influence of interlayer and support condition
  The comparison between the PVB and SG interlayers in Fig. 10(a) shows that when using SG, the sag branching was suppressed and the stresses generated at the edges and the center of the plane increased. This is attributed to the increased rigidity of the laminated glass when using SG. In the comparison between 4-point and 6-point supports in Fig. 10(b), the sag and generated stresses did not change much. In the legends A10, A11, B10, and B11, “A” indicates the outside surface, “B” indicates the inside surface, and the number indicates the strain measurement position in Fig. 3(a).

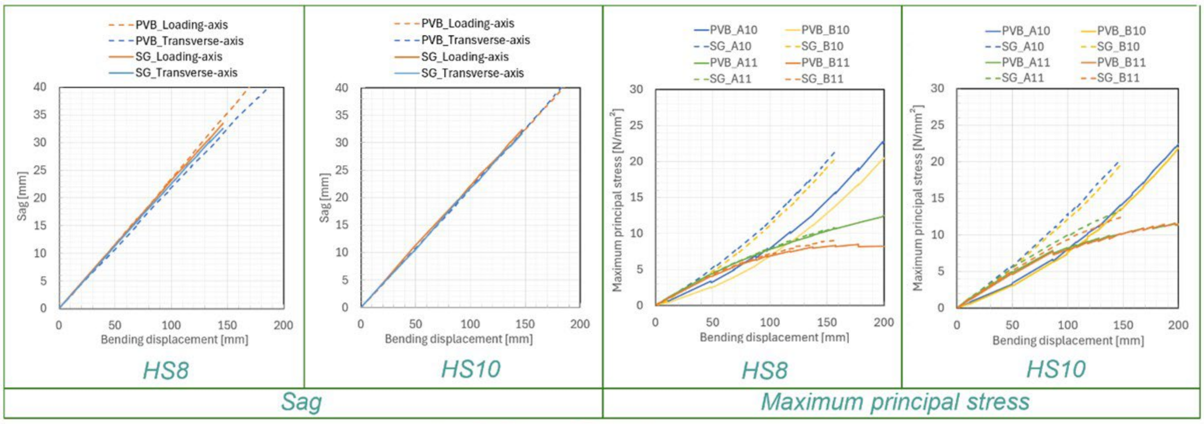

(a) PVB v.s. SG (4-line-support)

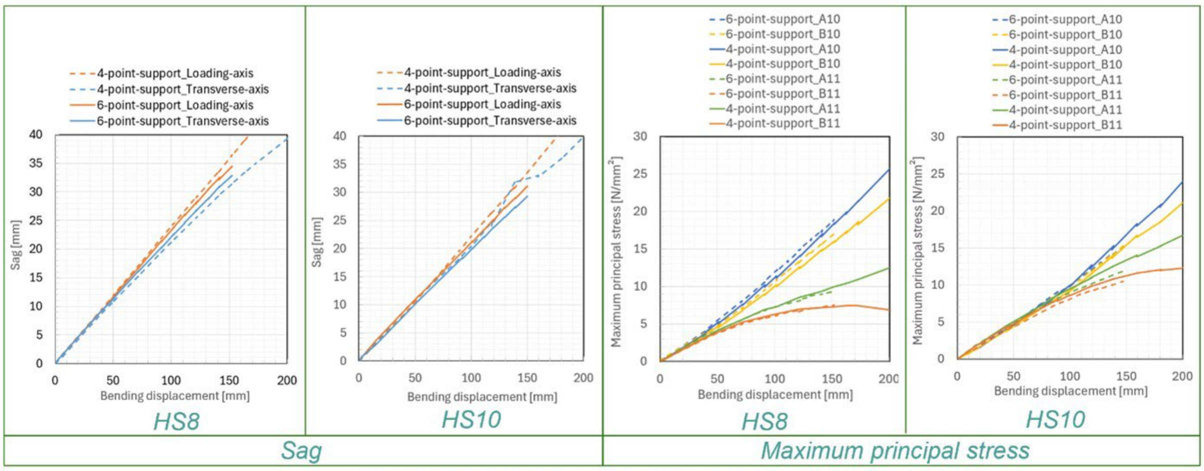

(b) 4-point-support v.s. 6-point-support (SG)

Fig. 10: Sag and maximum principal stress (interlayer type or support condition comparison).

- Out-of-plane deformation comparison between test and analysis
  A comparison of test and analysis results for out-of-plane deformation along the loading and transverse axes is shown in Fig. 11. The amount of bending displacement in the analysis was set to correspond to the test values. The analysis results mostly agree with the test results. The error is largest in the transverse axis of specimen No.5 because of the high non-linearity. The out-of-plane deformation of the loading and transverse axes is symmetrical when the bending displacement is small; however, at fracture, it becomes asymmetrical. In specimen No. 2, the transverse axis buckles, while in the other specimens, the loading axis buckles. It can be assumed that subtle initial imperfection determines which axis buckles, as noted in the study by Laurs et al. (2020). In the study, a uniformly distributed surface load of 0.0001 N/mm^2 was applied to initiate buckling. The out-of-plane deformation due to buckling occurred toward the direction of the initial imperfection. The buckling axis became more bent, and the sag was significantly enlarged. In contrast, the axis that did not buckle had a trapezoidal shape, indicating that the middle of the plane was bent back and straightened. The thinner the thickness of glass, the larger the distortion on the glass surface.

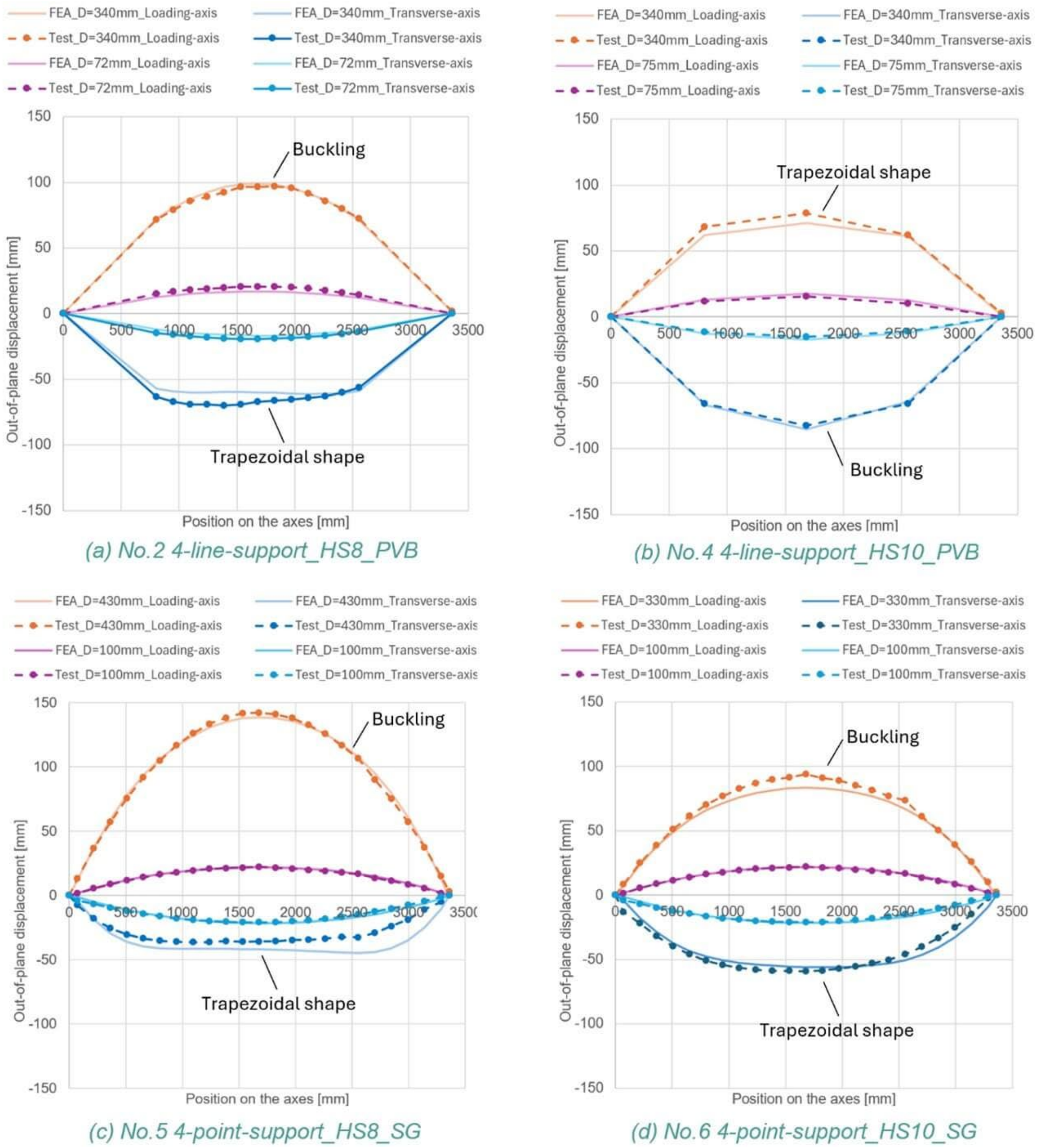

Fig. 11: Out-of-plane deformation comparison between test and analysis.

- Maximum principal stress comparison between test and analysis
  A comparison of test and analysis results for the maximum principal stress distribution is shown in Fig. 12. The test results were obtained by complementing the values of the measurement points (as shown in Fig. 3(a)). The distribution patterns and values of the maximum principal stress for all specimens closely correspond between the test and analysis results. In the case of 4-line support, the peak values of the maximum principal stresses occur in the center of the plane when the bending displacement is small, but near the center of the edges when the bending displacement is large. In the case of 4-point-support, the peak values of the maximum principal stresses occur locally around the loading point C and the opposite point A regardless of the amount of bending displacement. For both supports, the glass fracture origins obtained from the tests were in the range of high maximum principal stresses (test results shown in Fig. 5). In the plane located on the tensile side of the axis—which takes on a trapezoidal shape during buckling (as shown in Fig. 11)—the tensile stresses in the center of the plane decrease due to bending stresses that develop after buckling. Instead, the tensile stresses in the center of the plane on the other side inclease. The directions of the maximum principal stresses (red arrows in the test results of Fig. 12) were almost the same (almost 45 degrees) across the entire plane when the bending displacement was small, but as the bending displacement increased, the red arrows are enlarged and inclined nearly parallel to the edges.

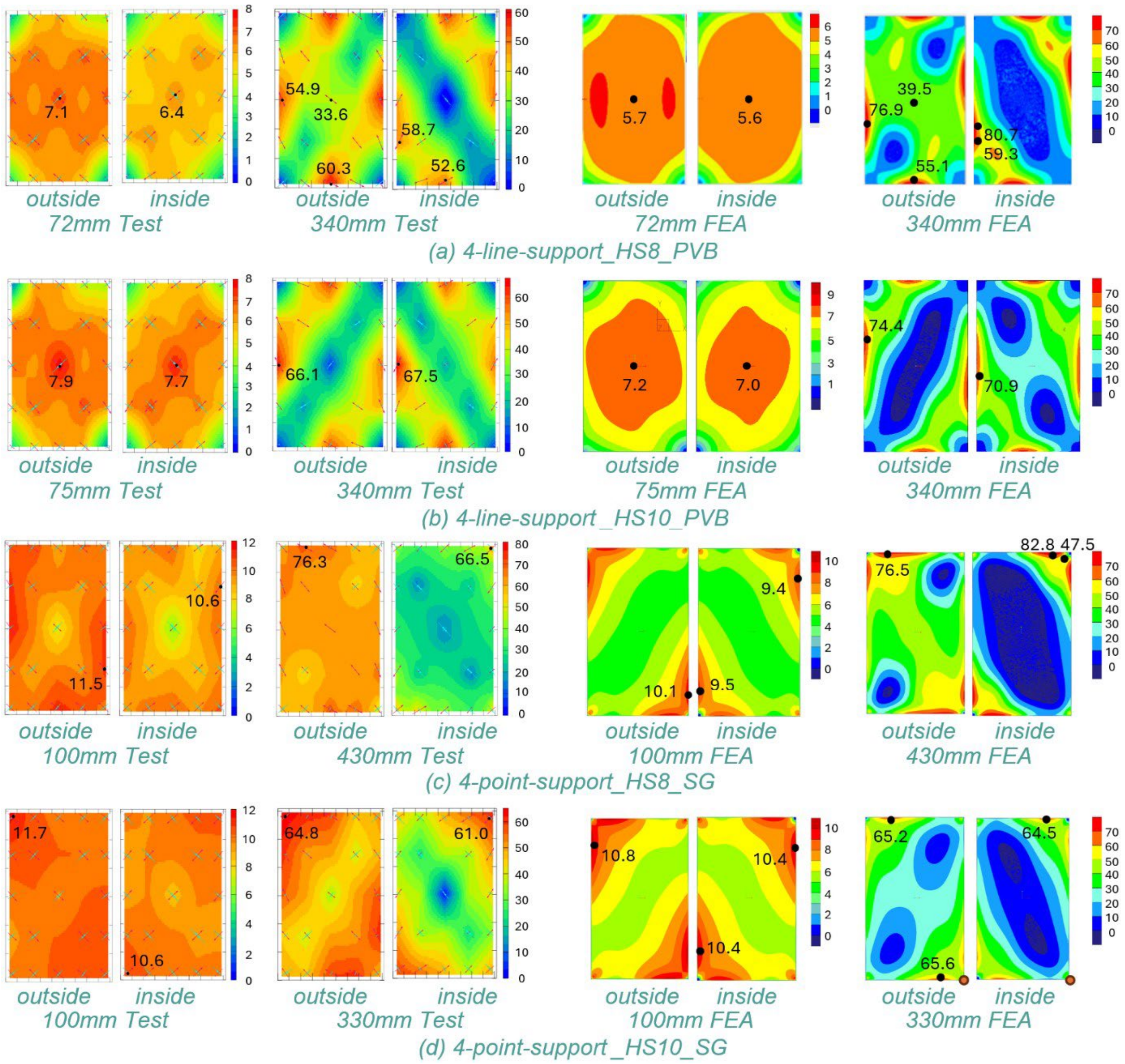

Fig. 12: Maximum principal stress distribution comparison between test and analysis (unit: N/mm²).

3. Wind load test and analysis of cold-bent glass

A wind load test was conducted on cold-bent glass to examine deformation and stress development.

- Outline of the test
  Figs. 13(a) and 13(b) show an overview of the test specimens. HS10+PVB 60mil+HS10 was used as the test specimen. It was placed vertically, with point B bent 90 mm outward, and an ideal uniform load was applied to the glass surface by an air chamber installed inside. The step of wind load pressure is shown in Fig. 13(c). After pre-pressure, wind load pressure was applied in steps of ±0.5 kPa until ±4.5 kPa was reached. Strain gauges were attached on both sides of the glass surface after cold bending was performed. The out-of-plane displacements of each marker attached to the outside surface was measured using a motion capture system, as described in section 2.

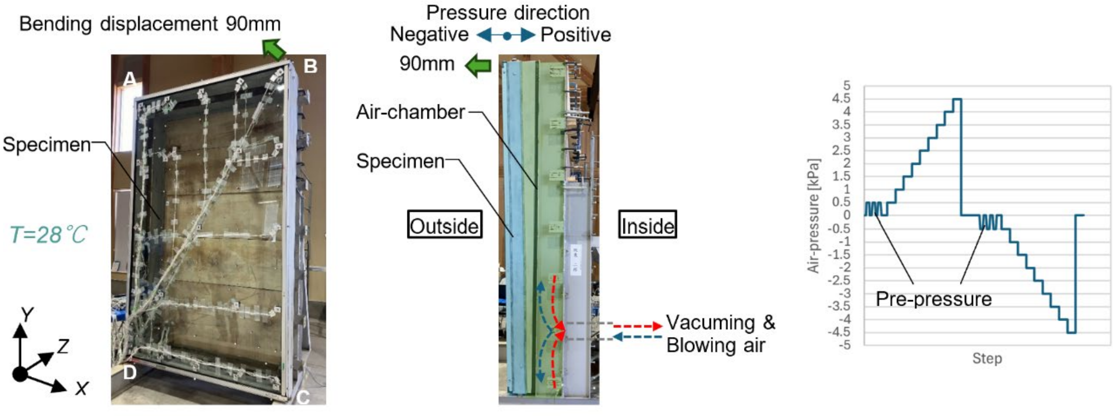

(a) front view *(b) side view* *(c) Loading step*

Fig. 13: Outline of the wind load test.

- Air-pressure and maximum principal stress
  The air-pressure–maximum and minimum principal stress relationship is shown in Fig. 14. In the small pressure range, the stress shows nearly linear behavior, but as the pressure increases, the slope of the graph decreases and becomes slightly non-linear. The stress generated on the compression side tends to be smaller than that on the tension side. The saddle shape of cold-bent glass is considered to affect geometric stiffness. Slight residual stresses were observed when the pressure was returned to 0 kPa. The snap-through buckling phenomenon reported by Quaglini et al. (2020) was not observed in this test. It is considered that this is because the 4-line-support / laminated glass has more resistance against the buckling than the 4-point-support / single glass.

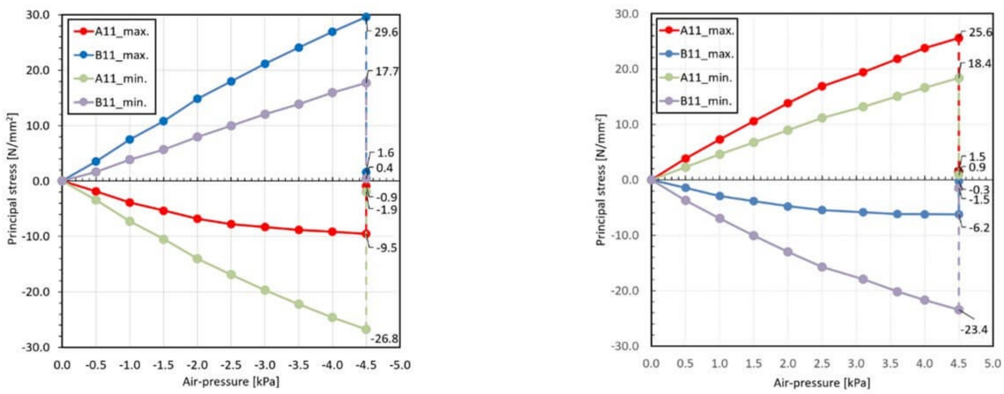

(a) positive direction *(b) negative direction*

Fig. 14: Air-pressure–maximum and minimum principal stress relationship (excluding the effect of cold-bent).

- Out-of-plane deformation
  The out-of-plane deformation of both axes is shown in Fig. 15. In the initial cold-bent condition with a wind pressure of 0 kPa, the sags of both axes are approximately 20 mm and nearly symmetrical. When subjected to a wind load of ±4.5 kPa, one axis experiences an increase in sag by approximately 20 mm (to about 40 mm) while the other experiences a decrease by approximately 20 mm (to about 0 mm). The FEA results shown by the solid lines correspond to the test results.

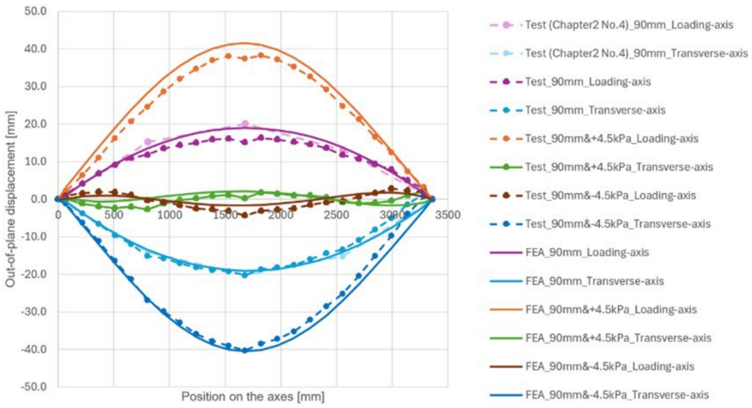

Fig. 15: Out-of-plane deformation of the loading and transverse axes under air-pressure.

- Distribution of maximum principal stress
  The maximum principal stress distribution is shown in Fig. 16, where the stress distributions from wind load and cold bending are superimposed. The stress contours are distorted by the cold bending, but the effect is limited. It should be noted that when wind load is applied to cold-bent glass, the stresses generated by both effects should be added in the center of the plane. The FEA and test results agree regarding the distribution patterns and generated stress values.

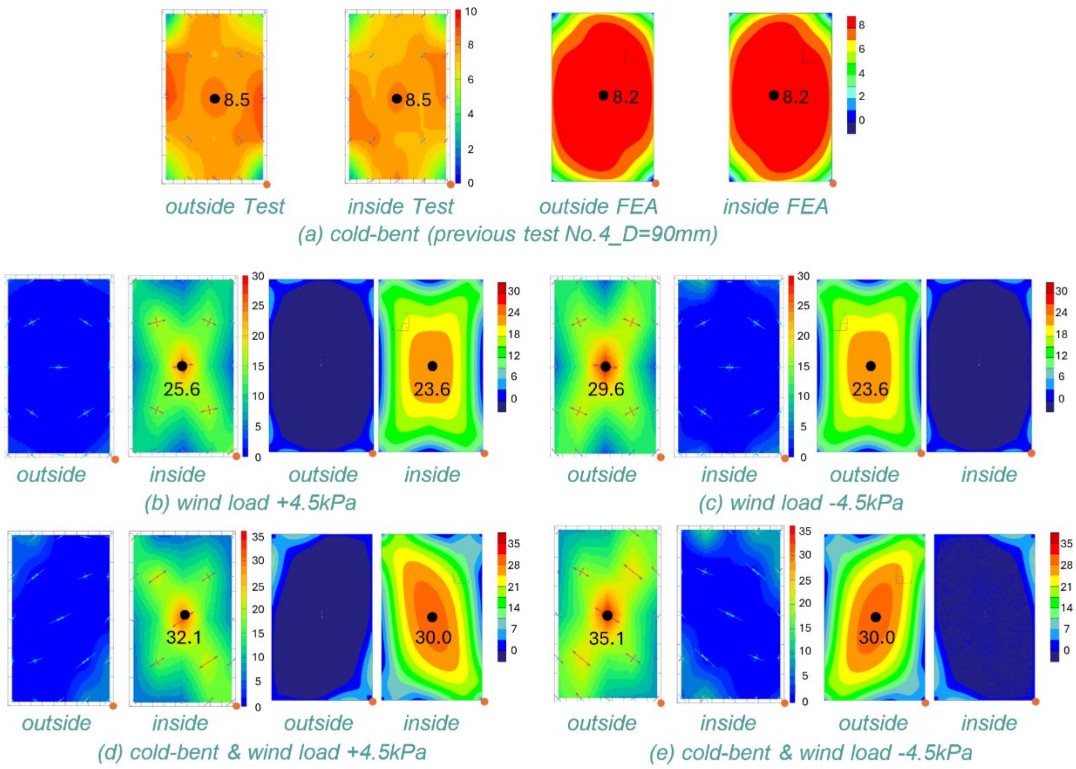

Fig. 16: Distribution of maximum principal stress (left side: test, right side: FEA, the position of the loading point and the direction of bending displacement were modified to match those of previous tests reported in section 2).

4. Relationship between Cold-bent displacement and edge stress

When bending displacement is applied to a glass corner, buckling or fracture occurs at some point. Previous studies (Datsiou (2017) and Galuppi et al. (2018)) focused on the degree of bending displacement at the point where the glass buckles, as optical distortion is considered to be the limit of use, and proposed a formula for evaluating the degree of bending displacement in rectangular glass when buckling occurs under 4-line-support. Not only buckling, Bensend (2016) examined the bending displacement corresponding to the allowable stress so that glass does not fracture and proposed a combined evaluation of buckling and fracture. Determining the stress limit is important because for a small and thick glass specimen, there are cases where the specimen may fail before buckling, particularly when using glass with low edge strength, such as float glass. Furthermore, when using glass with high strength, such as chemically strengthened glass, it may be bent beyond the buckling limit to the stress limit to maximize its performance. In this section, FEAs were conducted using the parameters of glass thickness, glass edge length (width and height), interlayer stiffness, interlayer thickness, and self-weight—focusing on the 4-line-support condition—to ascertain the degree of each influence. Subsequently, a fitting method using FEA results was used to derive an equation for bending displacement corresponding to edge-generated stress, taking into account the effects of glass thickness (t) and edge length (width (W) and height (H)), which have a high degree of influence.

- Influences of glass thickness t, glass width W, and glass height H

  The same deformation (D_{FEA} = 105.2 mm) was applied to laminated glass specimens with various thicknesses (t) and edge lengths (W and H). It was observed that increasing the plate thickness (t) and decreasing the edge lengths (W and H) resulted in larger edge-generated stress (σ_{FEA}).

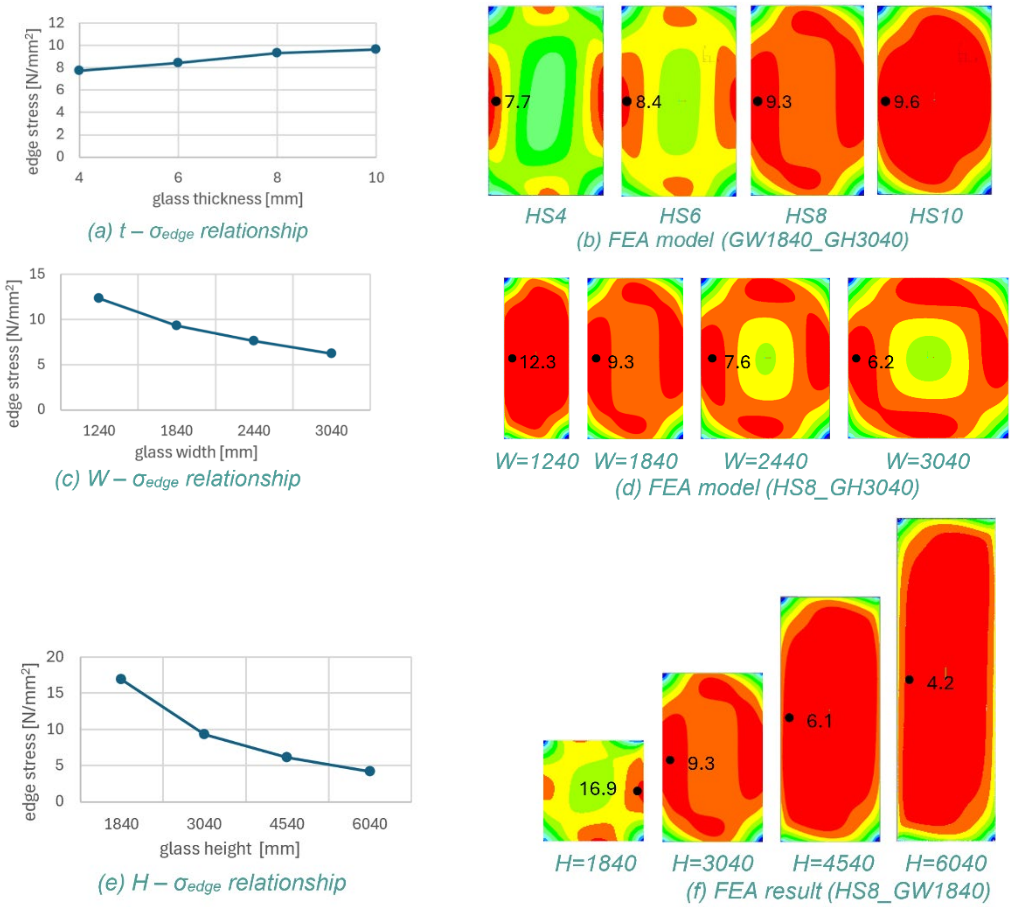

Fig. 17: Influence of (a, b): glass thickness t, (c, d): glass width W, (e, f): glass height H (unit: N/mm²).

- Influence of interlayer stiffness
  The same deformation (D_{FEA} = 105.2 mm) was applied to HS8 laminated glass with W = 1840 mm and H = 3040 mm. When the interlayer stiffness was less than approximately 10 N/mm², the edge stresses became constant as the glass layers acted independently; as the interlayer stiffness increased, the edge stresses tended to converge to a constant value as the glass layers acted as a composite unit. As the duration of the cold-bent load increases, the interlayer stiffness decreases. Thus, the generated stress settles down soon after the cold bending process is introduced, and the settled value is considered to be important for design calculations.

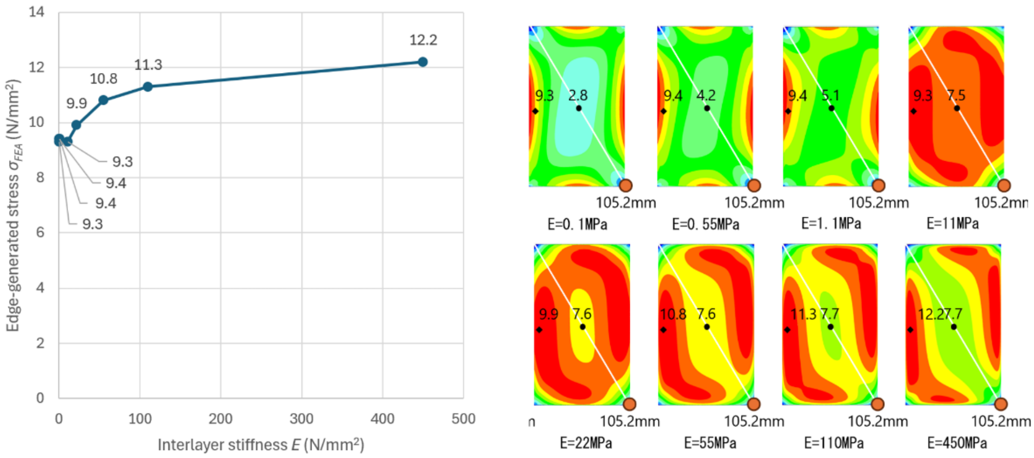

(a) Interlayer stiffness - edge stress relationship (b) FEA model (HS8_GW1840xGH3040)

Fig. 18: Influence of interlayer stiffness, unit: N/mm².

- Influence of interlayer thickness
  Analyses were conducted for commonly used interlayer thicknesses. The edge-generated stresses remained nearly the same, and the influence of the interlayer thickness was considered small.

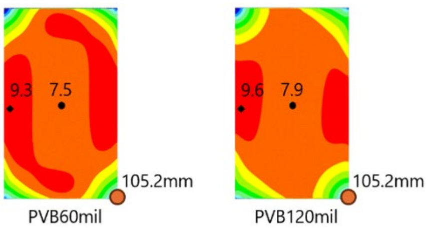

Fig. 19: Influence of interlayer thickness (HS8_1840 x 3040) (unit: N/mm²).

- Influence of gravity
  Although this study focuses on vertical installation, when installed horizontally the effect of self-weight should be added, similar to the wind load test mentioned in the previous section.

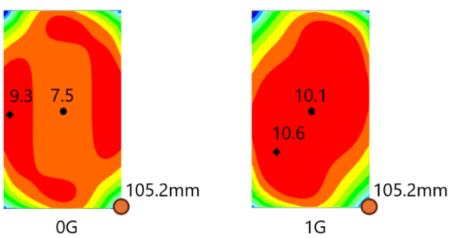

Fig. 20: Influence of gravity ±1G (HS8_1840 x 3040) (unit: N/mm²).

- Controlling the edge stress by calculated bent displacement

  The calculated bending displacement (D) is defined by Eq. (3) in a simple configuration, which is described as a four-variable function of the thickness (t), the edge lengths (W and H) and edge-generated stress (σ), considering the symmetry of W and H, and the effect of each non-linearities. And σ can be expressed as Eq. (4) by transforming Eq. (3). The σ_{FEA} for each FEA model was substituted into Eq. (3) to calculate D_{cal}, and five parameters (a, b, c, d, e) were determined so that D_{cal} fit to D_{FEA} in every FEA model cases. Fig. 21 shows the various FEA models used. Table 2 shows the fitted D_{cal} and $D_{Bensend}$, which is calculated using equations in study of Bensend (2016). D_{cal} agree with D_{FEA}, with an error within approximately ±10% regardless of t, W, and H, while $D_{Bensend}$ within approx. ±30%. Note that in this study, the five parameters were determined as follows:

$$a = 9.505 \times 10^{-4},\ b = 1.523,\ c = 0.8436,\ d = -0.1622,\ e = 0.6158$$

$$t_{eq} = 0.866 \times T - 0.268 \tag{2}$$

$$D = a \times (W^b + H^b)^c \times {t_{eq}}^d \times \sigma^e \tag{3}$$

$$\sigma = \left(D / \left(a \times (W^b + H^b)^c \times {t_{eq}}^d\right)\right)^{1/e} \tag{4}$$

T : total glass thickness [mm], W : glass width [mm], H : glass height [mm], t_{eq} : equivalent glass thickness [mm] of the Japanese guideline for PVB (t_{eq} = T when using SG for reference), *a, b, c, d, e* : *fitting parameters*, D: bending displacement [mm], σ: edge generated stress [N/mm^2], D_{cal}: calculated bending displacement using equation (3) [mm], $D_{Bensend}$: calculated bending displacement using equation in the study of Bensend (2016) [mm], D_{FEA}: FEA bending displacement [mm], σ_{FEA}: FEA edge generated stress [N/mm^2]

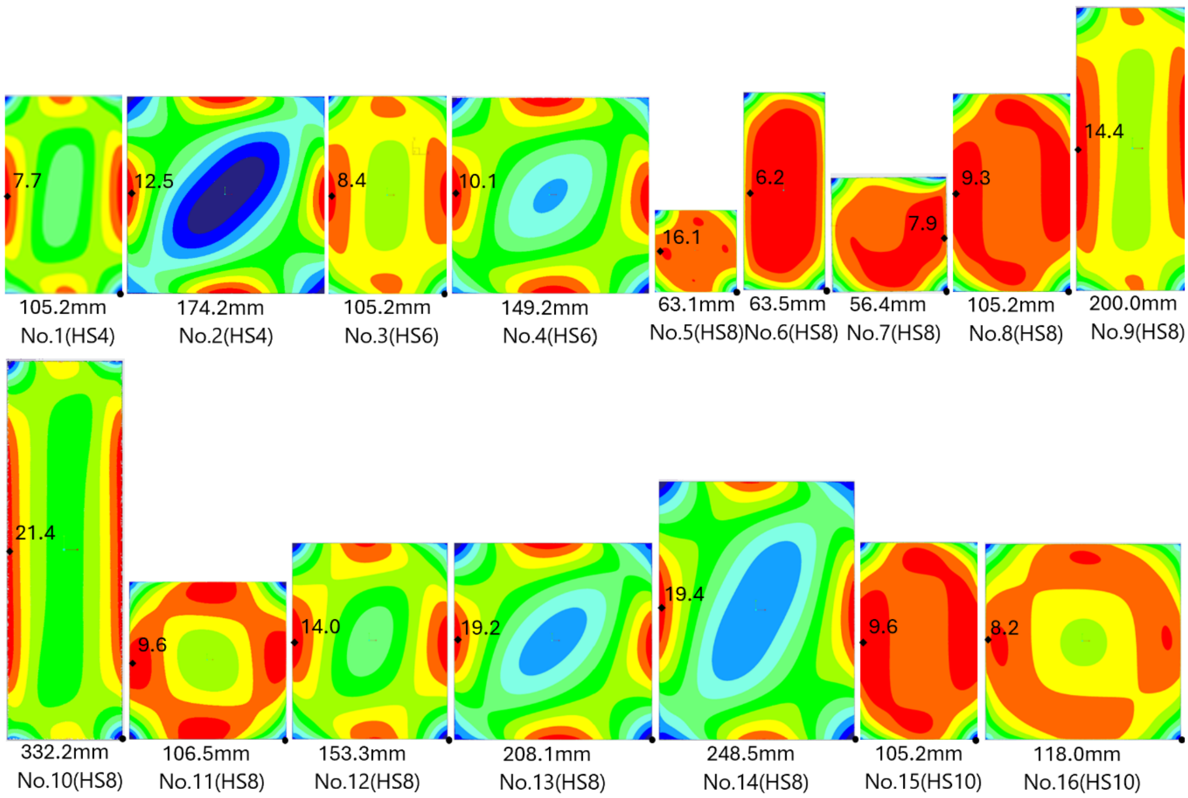

Fig. 21: Variation of FEA results used for fitting the parameters of the equation (unit: N/mm^2).

Table 2: The calculated value of bending displacement and maximum principal stress

No.	T [mm]	W [mm]	H [mm]	H/W -	t_{eq} [mm]	σ_{FEA} [N/mm^2]	D_{FEA} [mm]	D_{cal} [mm]	*Error* [%]	$D_{Bensend}$ [mm]	*Error* [%]
1	8	1840	3040	1.65	6.66	7.7	105.2	101.3	3.7	100.7	4.3
2	8	3040	3040	1.00	6.66	12.5	174.2	177.5	1.9	162.4	6.8
3	12	1840	3040	1.65	10.12	8.4	105.2	99.8	5.1	92.4	12.2
4	12	3040	3040	1.00	10.12	10.1	149.2	145.4	2.5	131.2	12.1
5	16	1240	1240	1.00	13.59	16.1	63.1	58.4	7.5	45.9	27.2
6	16	1240	3040	2.45	13.59	6.2	63.5	69.3	9.1	49.1	22.7
7	16	1840	1840	1.00	13.59	7.9	56.4	62.5	10.8	48.8	13.5
8	16	1840	3040	1.65	13.59	9.3	105.2	101.3	3.7	87.2	17.1
9	16	1840	4540	2.47	13.59	14.4	200	194.6	2.7	174.6	12.7
10	16	1840	6040	3.28	13.59	21.4	332.2	336.8	1.4	301.3	9.3
11	16	2440	2440	1.00	13.59	9.6	106.5	101.3	4.9	85.8	19.5
12	16	2440	3040	1.25	13.59	14.0	153.3	148.9	2.9	134.4	12.3
13	16	3040	3040	1.00	13.59	19.2	208.1	205.9	1.1	182.1	12.5
14	16	3040	4040	1.33	13.59	19.4	248.5	253.7	2.1	232.6	6.4
15	20	1840	3040	1.65	17.05	9.6	105.2	99.6	5.3	79.2	24.7
16	20	3040	3040	1.00	17.05	8.2	118	117.5	0.4	95.1	19.4

Fig. 22 shows the relationship between bending displacement and edge generated stress. D_{cal} is approx. 20% more conservative than D_{test} against the same amount of edge stress. D_{cal} is slightly closer to D_{test} compared to $D_{Bensend}$. Note that, the test results D_{test} of specimens No. 2 and No. 4 in section 2 correspond to the FEA results of No.8 and No.15 in Table 2, respectively. The nonlinear behavior after buckling can be expressed using the equation. Errors in a range of large bending displacement may be improved by fitting equation to analyses and tests more in that range.

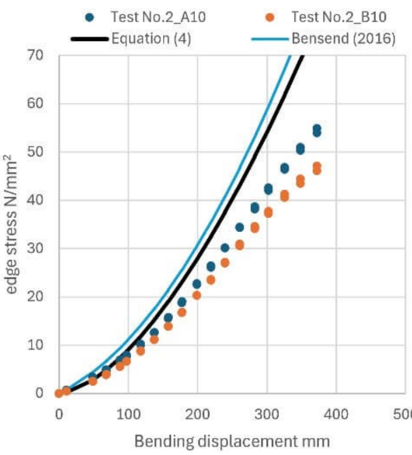

(a) Test No.2_4-line-support_HS8

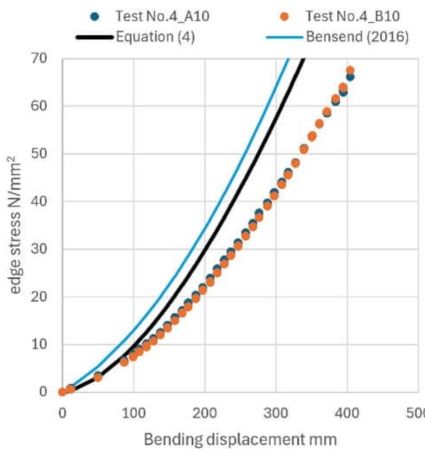

(b) Test No.4_4-line-support_HS10

Fig. 22: Bending displacement – edge stress relationship (comparison between equation and test conducted at section 2).

5. Conclusions

In this study, we conducted full-scale cold-bent glass fracture tests and finite element analyses (FEAs) to determine the fracture behavior, stress distribution, and effects of various parameters, such as the support conditions, glass thickness, and interlayer type. Additionally, wind load tests were conducted to evaluate the additional effects of cold bending. We also proposed an equation for determining the allowable bending displacement against stress. The following were found.

- Full-scale cold-bent glass breaking tests were conducted to confirm the fracture states. Glass fractures occurred when the bending displacement reached approximately 400 mm with GW1840 x GH3040 laminated glass. The fracture origins were found at the center of the long edge AD, opposite the loading point C in the case of a 4-line-support specimens, and near the support point A in the case of a 4-point-support specimens.
- The buckling phenomenon was observed as the bending displacement increased. Once buckling occurred, the glass took on an asymmetric shape, with the center bending more than the edges. However, while the edges exhibited less bending, tensile stresses increased.
- Comparison of glass thicknesses showed that thinner glass exhibited earlier and more prominent branching of both sag and maximum principal stress and a higher likelihood of buckling. Comparison of PVB and SG showed that SG tended to have less sag branching and higher generated stresses. Comparison of 4-point and 6-point support configurations showed little difference between the two in terms of sag and maximum principal stress.
- Wind load tests were conducted to examine the behavior of cold-bent glass under wind load. It was found that the stresses due to cold bending and wind load are superposed and need to be considered in design calculations. The stress distribution under wind load was distorted by cold bending, but the effect was small.
- A series of FEAs were conducted and found to be in good agreement with the test results in the cold-bent tests and the wind-load test. The validity of the FEA model was confirmed.
- An equation for bending displacement corresponding edge-generated stress, considering changes in glass thickness, width and height, was derived using FEAs.

References

Bensend, A. (2016). Maximizing the Twist of Cold Formed Glazing. Ghent, Belgium: Challenging Glass Conference, 5. Retrieved from https://doi.org/10.7480/cgc.5.2230

Datsiou, K. C. (2017). Design and Performance of Cold Bent Glass. Cambridge, UK: Apollo (University of Cambridge Repository). Retrieved from https://doi.org/10.17863/CAM.15628

Galuppi, L., Di Biase, P., Schaaf, B., Richter, C., Hoffmeister, B., Feldmann, M., & Royer-Carfagni, G. (2018). Hybrid steel-glass cell: cold-twisting and buckling phenomena. Delft, the Netherlands: Challenging Glass Conference, 6. Retrieved from https://doi.org/10.7480/cgc.6.2149

Laurs, M., Schaaf, B., Di Biase, P., & Feldmann, M. (2020). Numerical and Experimental Investigations on the Inherent Stress State of Cold-bent Glass. Ghent, Belgium: Challenging Glass Conference, 7. Retrieved from https://doi.org/10.7480/cgc.7.4503

Quaglini, V., Cattaneo, S., Pettorruso, C., & Biolzi, L. (2020). Cold bending of vertical glass plates: Wind loads and geometrical instabilities. England: Engineering structures, vol. 220. Retrieved from https://doi.org/10.1016/j.engstruct.2020.110983

Staaks, A.P. (2003). Koud torderen van glaspanelen in blobs (Cold Bent Glass Sheets in blobs). Eindhoven, German: Master thesis of Eindhoven University of Technology. Retrieved from Koud torderen van glaspanelen in blobs - Onderzoeksportaal Eindhoven University of Technology

Van Driel, T., Noteboom, C., & Overend, M. (2022). Investigations on the Cold Bending Behaviour of a Double Glazing Unit with a Rigid Edge-Spacer Frame. Ghent, Belgium: Challenging Glass Conference, 8. Retrieved from https://doi.org/10.47982/cgc.8.422